Magnetic Resonance Imaging of the Cavernous Sinus

David L. Daniels, Peter Pech, Leighton Mark, Kathleen Pojunas, Alan L. Williams and Victor M. Haughton

AJNR Am J Neuroradiol 1985, 6 (2) 187-192
http://www.ajnr.org/content/6/2/187

Magnetic Resonance Imaging of the Cavernous Sinus

David L. Daniels[1]
Peter Pech
Leighton Mark
Kathleen Pojunas
Alan L. Williams
Victor M. Haughton

The magnetic resonance (MR) appearance of the cavernous sinus was studied by correlating the MR images of normal volunteers and cryomicrotomic sections from six cadavers. In addition, MR images of patients with parasellar masses were compared with corresponding intravenously enhanced computed tomographic (CT) scans. The MR appearance of the cranial nerves in the cavernous sinuses is demonstrated, as well as MR signs of a parasellar mass, including obliteration of intracavernous venous spaces, displacement of the intracavernous internal carotid artery, and bulging of the lateral wall of the cavernus sinus. MR proved to be more effective than CT in delineating the parts of the cavernous sinus.

Magnetic resonance (MR) imaging has the potential to demonstrate the intracavernous segments of cranial nerves in contrast to the negligible signals of flowing blood. Our article describes the normal MR appearance of the cavernous sinuses and the MR signs of cavernous sinus lesions.

Materials and Methods

Six fresh frozen cadaver heads were embedded in styrofoam boxes with a solution of carboxymethyl cellulose gel. The orbitomeatal lines and sellae turcicae were identified with fluoroscopy. With a horizontally cutting heavy-duty sledge cryomicrotome (LKB 2250) and serial photography of the surfaces of the specimens [1], anatomic images of the cavernous sinuses were obtained in planes parallel or perpendicular to the orbitomeatal line. In the anatomic images, the intracavernous segments of cranial nerves III–VI and of the internal carotid arteries (ICAs) were identified using published anatomic, computed tomographic (CT), and MR literature [2–6].

A group of seven normal volunteers and 15 patients were chosen for MR imaging. The patients included two with pituitary adenomas involving cavernous sinuses and one with a parasellar aneurysm. The diagnoses were verified with conventional clinical, CT, angiographic, and surgical (two cases) findings.

The volunteers and patients were studied in prototype 1.3, 1.4, or 1.5 T General Electric MR scanners. Initially, a partial saturation (PS) sagittal image was used to determine locations for axial and coronal PS, inversion recovery (IR), and spin-echo (SE) imaging. Sections parallel (axial plane) and/or perpendicular (coronal plane) to the orbitomeatal line were obtained. Sequences included PS (300–500 msec TR, one or two averages, 128 × 256 or 256 × 256 matrix, and 3, 5, or 10 mm slice thickness); PS in a prospective zoom mode in which the field of view was reduced to 12.5 cm (400–500 msec TR); IR (1500 msec TR, 600 msec TI, one average, 128 × 256 matrix, and 5-mm-thick slices); and SE (2000 msec TR, 25, 50, 75, and 100 msec TEs, 128 × 256 matrix, one average, and 5-mm-thick slices). Axial and coronal MR images of the patients were compared with cryomicrotomic sections to identify cranial nerves in the cavernous sinus. MR images of patients with parasellar masses were correlated with corresponding intravenously enhanced CT images made on CT/T 8800 or 9800 scanners with conventional radiographic factors.

This article appears in the March/April 1985 issue of *AJNR* and the May 1985 issue of *AJR*.

Presented at the annual meeting of the American Society of Neuroradiology, Boston, June 1984.

This work was supported by a grant from General Electric Medical Systems.

[1] All authors: Department of Radiology, Medical College of Wisconsin, Froedtert Memorial Lutheran Hospital, 9200 W. Wisconsin Ave., Milwaukee, WI 53226. Address reprint requests to D. L. Daniels.

***AJNR* 6:187–192, March/April 1985**
0195–6108/85/0602–0187

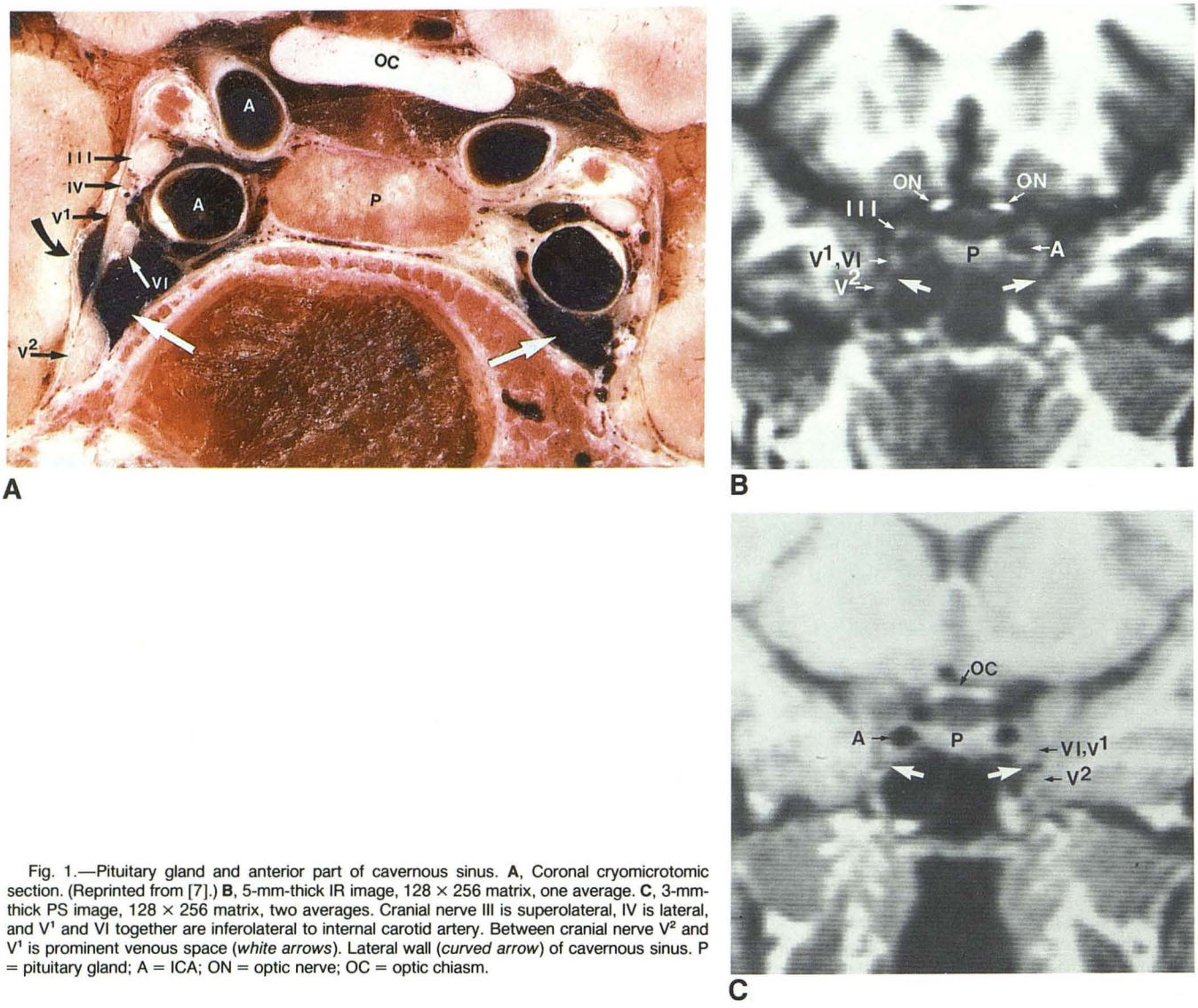

Fig. 1.—Pituitary gland and anterior part of cavernous sinus. **A**, Coronal cryomicrotomic section. (Reprinted from [7].) **B**, 5-mm-thick IR image, 128 × 256 matrix, one average. **C**, 3-mm-thick PS image, 128 × 256 matrix, two averages. Cranial nerve III is superolateral, IV is lateral, and V^1 and VI together are inferolateral to internal carotid artery. Between cranial nerve V^2 and V^1 is prominent venous space (*white arrows*). Lateral wall (*curved arrow*) of cavernous sinus. P = pituitary gland; A = ICA; ON = optic nerve; OC = optic chiasm.

Results

The important landmarks of the cavernous sinus in axial and coronal cryomicrotomic sections are cranial nerves III–VI, the gasserian ganglion in Meckel cave, the ICA, and the lateral wall of the cavernous sinus. The coronal cryomicrotomic sections show that the cranial nerves in the cavernous sinuses have a constant position with respect to the ICA (fig. 1). Cranial nerve III is superolateral to the artery, cranial nerve IV (which is much smaller than III) is lateral, and cranial nerves V^1 and VI together are inferolateral. A prominent venous space and cranial nerve V^2 below it are at the inferior aspect of each cavernous sinus. Coronal cryomicrotomic sections through the posterior part of the cavernous sinus show cranial nerves III and IV and Meckel cave lateral to the ICA (figs. 2 and 3).

The coronal PS or IR images with slice thickness of 3 or 5 mm show small foci of high-intensity signals that correspond to cranial nerves III, V^1, V^2 and VI in the cavernous sinuses (figs. 1 and 4). The intensity of the signals is approximately equal to that of the corpus callosum. Adjacent flowing blood produces negligible signals. The nerves (especially cranial nerve III) are better defined on a PS image using a zoom technique (fig. 4). The venous space between V^1 and V^2 appears as a region of negligible signals. In coronal PS sections through the posterior aspect of the cavernous sinus, Meckel cave appears as an oval-shaped region with slightly greater signal intensity than cerebrospinal fluid (CSF) (figs. 2 and 3).

In 5-mm-thick coronal SE images, cranial nerves V^1, V^2, and VI have high-intensity signals (fig. 4). The venous space above V^2 has negligible signals. Cranial nerves III and IV are not confidently identified.

Meckel cave has a low- or high-intensity signal depending on the pulse sequences. In T2-weighted images (late echoes in SE images) it has an intense signal; in T1-weighted images (PS) it has a low intensity signal. In axial images individual

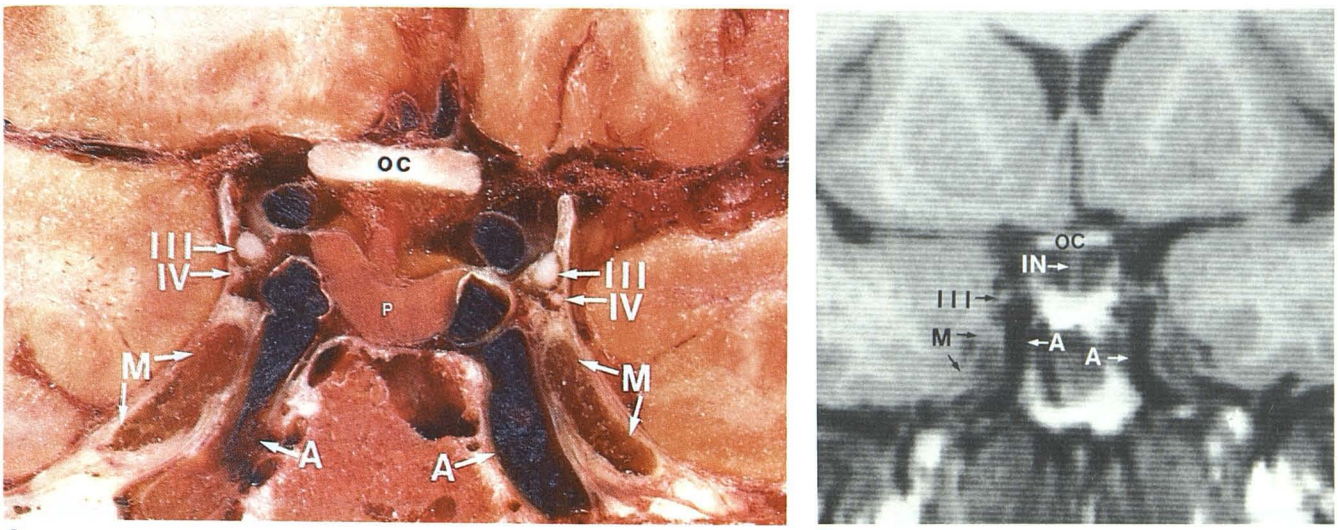

Fig. 2.—Posterior to fig. 1. **A**, Coronal cryomicrotomic section. Meckel cave (M) is lateral to vertical segment of ICA (A). **B**, 3-mm-thick PS image, 256 × 256 matrix, two averages. Meckel cave is oval area of low signal intensity. Cranial nerve III is identified. IN = infundibulum; OC = optic chiasm; P = pituitary gland. (Reprinted from [7].)

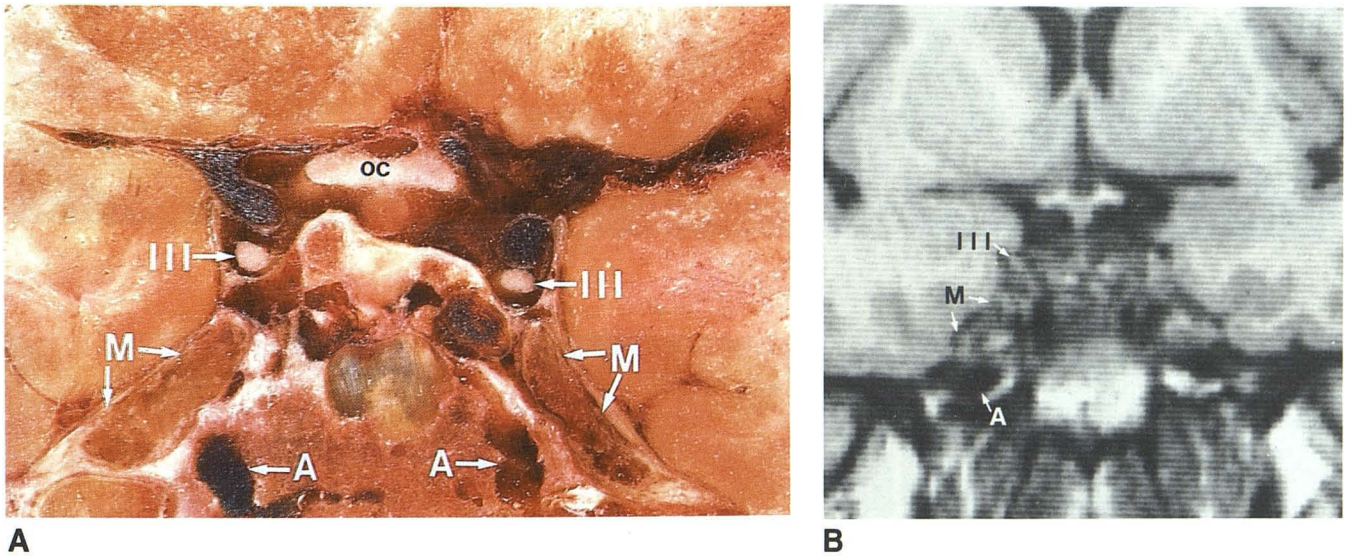

Fig. 3.—Posterior to fig. 2. **A**, Coronal cryomicrotomic section. B, 3-mm-thick PS image, 256 × 256 matrix, two averages. Meckel cave (M) has slightly less intense signal than cranial nerve III. OC = optic chiasm; A = internal carotid artery. (Reprinted from [7].)

cranial nerves in the cavernous sinuses are not differentiated (fig. 5). In T2-weighted images, high-intensity signal from CSF is detected lateral to the lateral wall of the cavernous sinus, while in PS images the CSF and the lateral wall both have low-intensity signals (fig. 5C). The lateral wall appears either straight or curving slightly concavely.

Masses in the cavernous sinus were clearly demonstrated in the MR studies (figs. 4, 6, and 7). A parasellar mass obliterated the venous space above cranial nerve V^2, obscured the cranial nerves on coronal MR images, and usually produced bulging of the lateral wall of the involved cavernous sinuses. Tumor producing a greater signal intensity than the blood in the cavernous sinuses or ICAs was easily detected when it encroached on these structures. In one case displacement of the carotid artery was demonstrated; in the other encasement of the carotid artery was demonstrated.

Discussion

MR demonstrates the cranial nerves effectively. Cranial nerves VII and VIII can be identified on a PS sequence because they are surrounded by low-intensity signals from

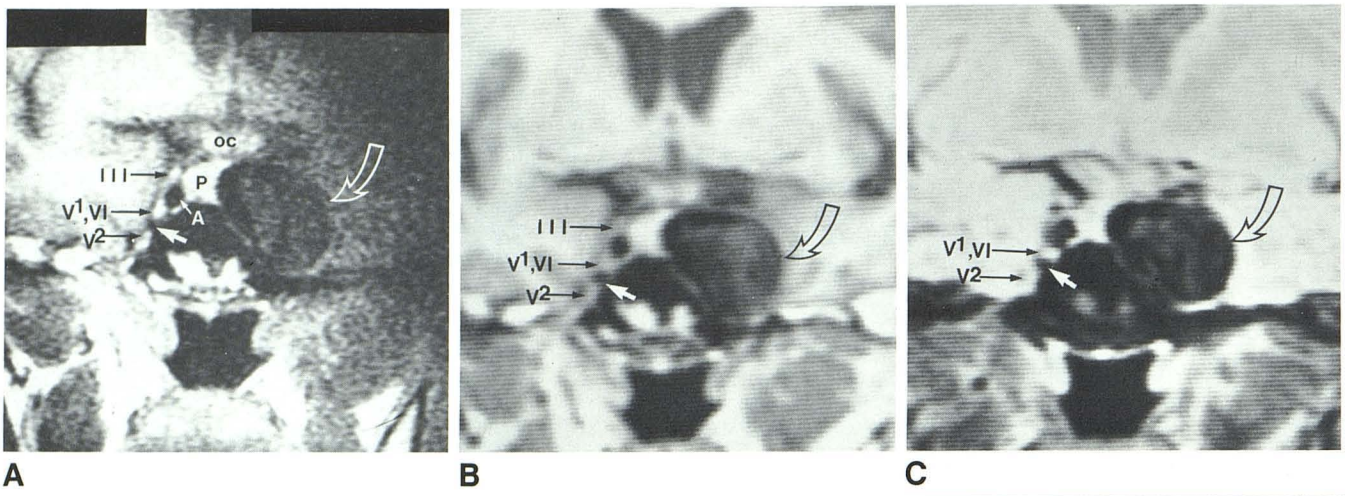

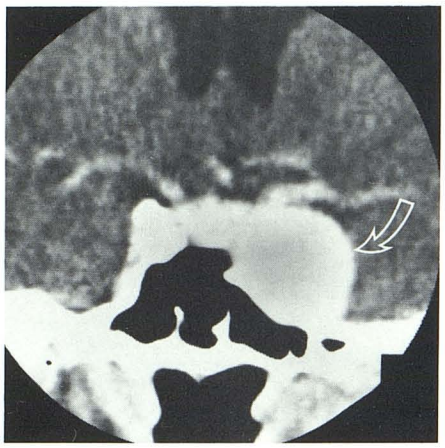

Fig. 4.—Coronal images of left parasellar aneurysm deforming pituitary gland. **A**, 5-mm-thick PS zoom image, 128 × 256 matrix, four averages. **B**, PS image, 128 × 256 matrix, two averages. **C**, SE image, 128 × 256 matrix, one average. **D**, Enhanced CT scan. Aneurysm (*curved arrows*) enhances homogeneously in **D** but has inhomogeneous MR signals, probably because of turbulent blood flow. Cranial nerves in right cavernous sinus have high-intensity signals. Prominent venous space (*closed arrows*) above cranial nerve V^2 has negligible signals. OC = optic chiasm; P = pituitary; A = ICA. (**B** reprinted from [7].)

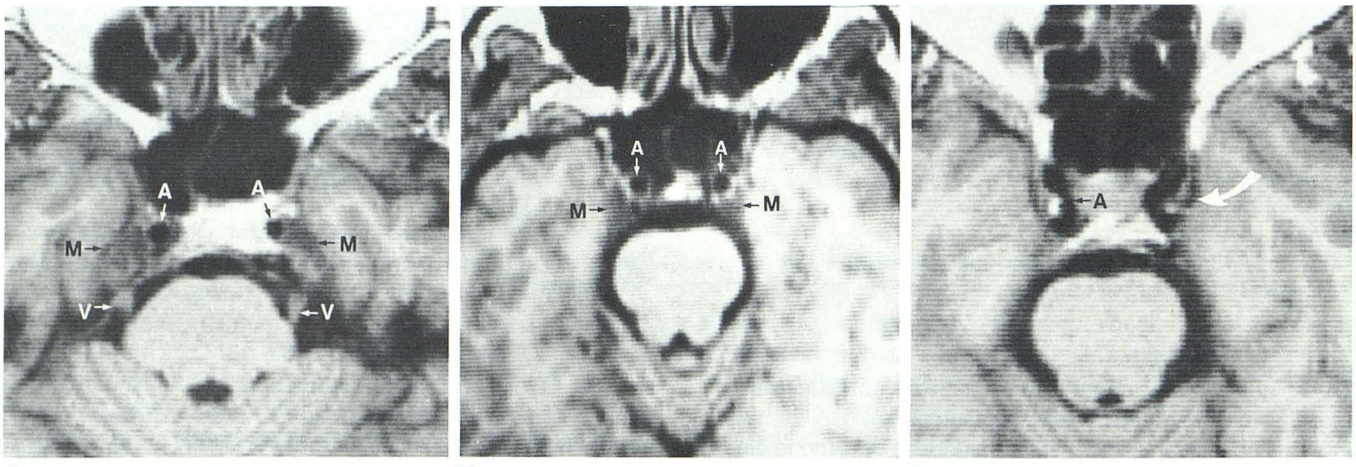

Fig. 5.—Progressively more rostral axial images. **A** and **B**, 3-mm-thick PS images, 256 × 256 (**A**) and 128 × 256 (**B**) matrices, two averages each. Meckel cave (M) has slightly greater signal intensity than CSF. **C**, 3-mm-thick PS image, 256 × 256 matrix, two averages. Lateral wall of cavernous sinus and adjacent CSF have negligible signal (*arrow*). A = ICA. (**A** and **C** reprinted from [7].)

either the CSF or the petrous bone [8]. Cranial nerves III, V^1, V^2, and VI in the cavernous sinus also can be shown with MR because they are surrounded by low-intensity signal from flowing blood. We were unable to image cranial nerve IV in the cavernous sinus, probably because of its small size and close proximity to cranial nerve III.

MR demonstrates the contents of the cavernous sinuses more effectively than CT does. With MR the carotid arteries,

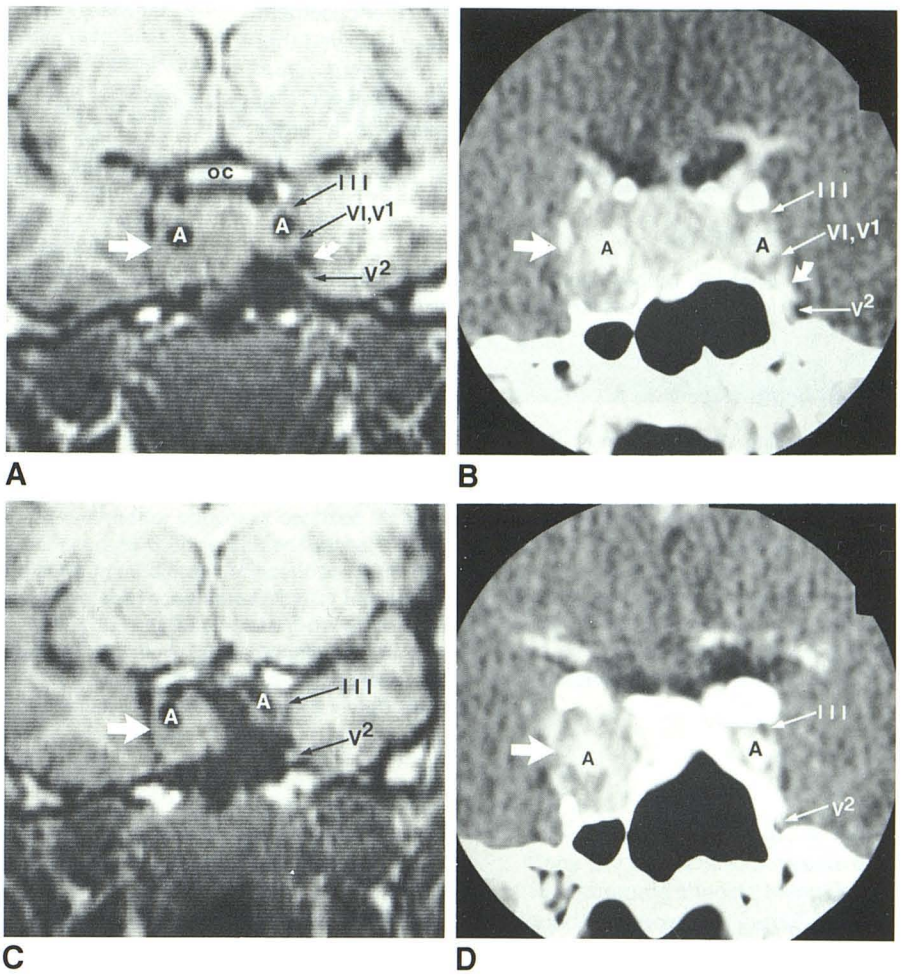

Fig. 6.—Prolactinoma extending laterad (*straight arrows*), encasing right ICA, and obscuring cranial nerves in right cavernous sinus. Corresponding coronal 3-mm-thick PS image, 128 × 256 matrix, two averages (**A**), and enhanced CT scan (**B**). Cranial nerves III and V^1 plus VI are adjacent to left ICA, and venous space (*curved arrows*) is above V^2. More anterior, 3-mm-thick PS image, 128 × 256 matrix, two averages (**C**), and enhanced CT scan (**D**). V^2 in left foramen rotundum. OC = optic chiasm; A = ICA.

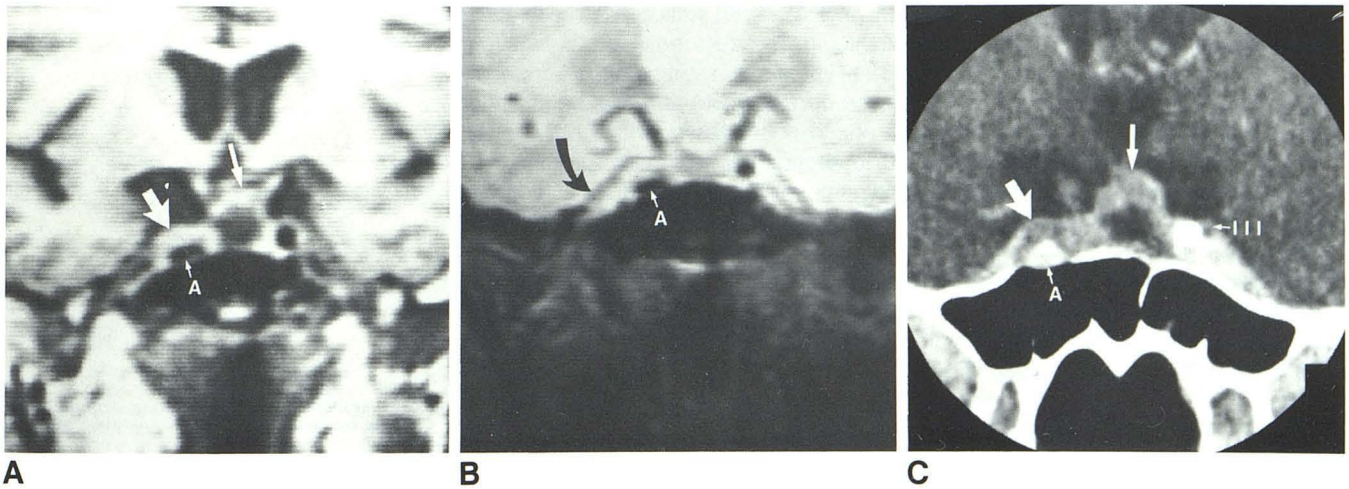

Fig. 7.—Partly cystic pituitary adenoma (*thin arrow*) extending to right cavernous sinus (*thick arrow*). **A**, 5-mm-thick PS image, 128 × 256 matrix, two averages. **B**, SE image, 128 × 256 matrix, one average. **C**, Enhanced CT scan. Tumor displaces right ICA (A) but not lateral cavernous sinus wall (*curved arrow*).

cranial nerves, and vascular channels in the cavernous sinus can be resolved consistently, while CT often fails to show vascular structures in the cavernous sinuses unless dynamic scanning techniques are used. The anatomic landmarks in MR studies, including cranial nerves III, V^1, and V^2, the venous space between V^1 and V^2, and the carotid artery, can be used to detect masses encroaching on the cavernous sinuses. Therefore MR has greater sensitivity than CT for detecting

tumor encroachment on the cavernous sinus or encasement or displacement of the carotid artery. Our cases showed that tumor has a greater signal intensity than cavernous sinus blood. The specificity and sensitivity of MR versus CT in cavernous sinus pathology can be determined in a larger series of patients.

ACKNOWLEDGMENTS

We thank Cheryl D. Tauber, Laurie A. Dunk, Peggy Dreifke, Linda Hutten, and Janice Alba for assistance in performing this study.

REFERENCES

1. Rauschning W, Bergstrom K, Pech P. Correlative craniospinal anatomy studies by computed tomography and cryomicrotomy. *J Comput Assist Tomogr* **1983**;7:9–13
2. Umansky F, Nathan H. The lateral wall of the cavernous sinus. *J Neurosurg* **1982**;56:228–234
3. Harris FS, Rhoton AL. Anatomy of the cavernous sinus, a microsurgical study. *J Neurosurg* **1976**;45:169–180
4. Kline LB, Acker JD, Post MJD, Vitek JJ. The cavernous sinus: a computed tomographic study. *AJNR* **1981**;2:299–305
5. Segall HD, Ahmadi J, McComb JG, Zee CS, Becker TS, Han JS. Computed tomographic observations pertinent to intracranial venous thrombotic and occlusive disease in childhood. *Radiology* **1982**;143:441–449
6. Hawkes RC, Holland GN, Moore WS, Corston R, Kean DM, Worthington BS. The application of NMR imaging to the evaluation of pituitary and juxtasellar tumors. *AJNR* **1983**;4:221–222
7. Daniels DL, Pojunas KW, Pech P, Haughton VM. *Magnetic resonance imaging of the sella and juxtasellar region.* Milwaukee: General Electric, **1984**
8. Daniels DL, Herfkens R, Koehler PR, et al. Magnetic resonance imaging of the internal auditory canal. *Radiology* **1984**;151:105–108